A modal H_∞-norm-based performance requirement for damage-tolerant active controller design

Helói F.G. Genari [a,b,*], Nazih Mechbal [b], Gérard Coffignal [b],
Eurípedes G.O. Nóbrega [a]

[a] Department of Computational Mechanics, University of Campinas, Campinas, Brazil
[b] Laboratory of Process and Engineering in Mechanics and Materials, Arts et Métiers ParisTech, Paris, France

ABSTRACT

Damage-tolerant active control (DTAC) is a recent research area that encompasses control design methodologies resulting from the application of fault-tolerant control methods to vibration control of structures subject to damage. The possibility of damage occurrence is not usually considered in the active vibration control design requirements. Damage changes the structure dynamics, which may produce unexpected modal behavior of the closed-loop system, usually not anticipated by the controller design approaches. A modal H_∞ norm and a respective robust controller design framework were recently introduced, and this method is here extended to face a new DTAC strategy implementation. Considering that damage affects each vibration mode differently, this paper adopts the modal H_∞ norm to include damage as a design requirement. The basic idea is to create an appropriate energy distribution over the frequency range of interest and respective vibration modes, guaranteeing robustness, damage tolerance, and adequate overall performance, taking into account that it is common to have previous knowledge of the structure regions where damage may occur during its operational life. For this purpose, a structural health monitoring technique is applied to evaluate modal modifications caused by damage. This information is used to create modal weighing matrices, conducting to the modal H_∞ controller design. Finite element models are adopted for a case study structure, including different damage severities, in order to validate the proposed control strategy. Results show the effectiveness of the proposed methodology with respect to damage tolerance.

1. Introduction

Active vibration control has become increasingly important due to the current demand of light and flexible structures for engineering systems. These structures are more susceptible to damage, which results from different factors such as fatigue, impact, and environmental caused stress. For some decades, a significant number of vibration control methods, with different success degrees, have been developed [1–7]. However, these methods rarely take into account structural damage as design requirements. To overcome controller performance decline due to damage, this paper presents a methodology to design damage-tolerant active controllers, based on the modal H_∞ norm. This constitutes a multidisciplinary methodology,

---

merging concepts of vibration control, modal control, fault-tolerant control, and structural health monitoring in order to cope with structural damage effects.

Damage-tolerant active control (DTAC) is a research area arisen from intense investigation to bring more secure and efficient operation to flexible structures, aiming for extension of their life cycle as well [8]. DTAC strategies were recently proposed by Mechbal and Nóbrega [9], merging concepts of vibration control and fault-tolerant control areas. The first goal of DTAC methods is to achieve an adequate performance for healthy real-life structures. For this purpose, DTAC systems need to be able to solve the regular active control problem, which involves avoiding the spillover phenomenon [10] and, for the sake of realism, adopting noncollocated transducers on mechanical structures [11]. In addition, as a second goal, the controlled system should prevent or retard damage occurrence. This basic DTAC idea corresponds to reducing vibration of the known damaging modes subject to stress conditions. In case of structural damage, the third goal is that the controller should act to mitigate damage effects on structural vibrations, avoiding or delaying damage propagation [12].

Mechanical structures have an infinite number of vibration modes, implying that a reduced model with a manageable order should be chosen in order to design the controller. The spillover phenomenon corresponds to the undesired excitation of the structure neglected dynamics. This phenomenon may lead the controlled system to instability if it is not properly considered during the design phase [13–15]. Some possible solutions are to use a smart structure with a large number of collocated transducers [16] or to include in the collocated structure model a constant feed-through term to represent the effects of the neglected dynamics on low-frequency zeros [17]. In many applications such as monitoring aeronautical structures, the collocated approach is not a realistic solution because placing a large number of sensors and actuators in the same locations may be impractical and eventually impossible due to the inaccessibility of some structure regions. In consequence, the development of control techniques for noncollocated mechanical structures has become a relevant research theme [18–20]. However, noncollocated systems have in general some zeros on the right half-plane, rendering a more complex structure dynamics to control [21–23].

Performance and robustness of vibration control techniques are dependent on model accuracy [24,25]. Damage produces structural dynamic changes, implying additional model uncertainties [26]. Therefore, most control methods do not guarantee an acceptable performance after a damage occurrence. H_∞-based control methods are able to handle model uncertainties, parameter variations, and the spillover phenomenon, attenuating low-order vibration modes successfully without excitation of out-of-interest bandwidth natural frequencies. For this purpose, weighing filters are used to avoid the spillover phenomenon and to obtain a reasonable trade-off between performance and robustness [27]. However, mode selectivity in terms of both the amplitude and the frequency in the interest bandwidth is usually a difficult objective because H_∞ control techniques work with contiguous low-frequency bands. Common modal control techniques provide reasonable modal selectivity, but these methods are still very sensitive to spillover [28–32].

Recently, Genari et al. [33] introduced a new control method associating modal control and H_∞ control concepts, aiming to achieve higher performance through modal selectivity. A modal H_∞ norm was proposed and used to specify the controller behavior, which conducts to a good modal selectivity in relation to regular modal controllers. The control strategy is to design a modal robust controller that achieves an adequate performance through the vibration reduction of high energy modes, controlling each mode independently. This control methodology was examined in structures undergoing damage, obtaining promising simulated and experimental results. However, modes with lower energy can also be affected by damage, eventually leading to a significant vibration increase of the controlled structure. To overcome this limitation, the strategy proposed here is based on the modal H_∞ control approach, in order to create an appropriate energy distribution throughout the vibration modes, taking into account the damage effect on each mode. A structural health monitoring (SHM) module assesses the damage severity on each mode. Considering the expected damage information, modal weighing matrices are built and used to design the new controller, using a linear matrix inequality (LMI) approach. The proposed strategy is evaluated in terms of robustness and vibration rejection and is compared to the regular H_∞ control technique. The studied structure is a flexible beam with noncollocated piezoelectric transducers, modeled through the finite element (FE) method. An increasing severity damage is simulated to test and compare the controller performances.

This paper is organized as follows: in Section 2, the adopted DTAC strategy is presented; in Section 3, the state-space model of a flexible structure is defined, in which the modal representation is introduced; in Section 4, the modal H_∞ norm is presented and the modal control is written as an equivalent regular H_∞ control problem; in Section 5, a modal damage indicator is proposed and is used to build the modal weighing matrices; in Section 6, the validation of the modal H_∞ control technique for DTAC applications is conducted, where the simulated results with FE models are analyzed, and final remarks are then presented in the last section.

2. Adopted damage-tolerant active control strategy

DTAC strategies are based on the structure state condition, depending on whether the structure is healthy or damaged [9]. For the healthy structure condition, Mechbal and Nóbrega [8] have proposed the following strategies:

- strictly tolerant active control;
- preventive active control.

The strictly tolerant active control represents a classic approach based on a nonreconfigurable controller with enough robustness, aiming to guarantee an acceptable performance for some types and severity levels of damage. However, the compromise between robustness and performance may lead the control system to unsatisfactory behavior in damage absence because these features are opposite to each other. To overcome this limitation, Genari et al. [33] proposed a robust modal approach that leads to a reasonable compromise between robustness and performance, in which the healthy structure and the damaged structure have an adequate performance level with the same controller.

The preventive active control strategy consists in designing controllers to avoid or to retard damage occurrence, aiming to extend structure life. For instance, Chomette et al. [25] designed a controller that attenuates most damaging modes. Ambrosio et al. [34] included material fatigue in a cost function, which is then minimized to obtain the preventive controller.

If the damage is identified, Mechbal and Nóbrega [8] have proposed two other possible strategies to be applied:

- evolving damage active control;
- adaptive tolerant active control.

The evolving damage active control strategy supposes that damage is detected, localized, and quantified. The controller is designed to limit damage propagation, acting to reduce vibration energy flow to the damaged region. This strategy is elaborated to design controllers that act locally such as the spatial approach and the distributed control. For instance, the spatial H_∞ methodology applied to structural damage control was investigated in [8].

The adaptive tolerant active control approach goal is to detect and to accommodate damage and, at the same time, to provide an adequate performance level for the control system. For this purpose, an SHM module and an adaptive controller are used to compose the control system. Thus, considering that the controller objective is to mitigate damage effects, the SHM module should detect the damage and signal the controller to be reconfigured according to the SHM data. The adaptive strategy was used by Mechbal and Nóbrega [12] to build a control system tolerant to damage. For this purpose, an SHM module based on Lamb wave method was used to localize damage. Then, the spatial H_∞ controller was reconfigured to reduce vibration energy flow in the damaged region. Ripamonti et al. [35] have proposed an adaptive strategy to improve the fatigue life of smart structures, based on an identification process, which provokes a switch between a fixed LQR controller, designed for the healthy structure, or an adaptive one. The respective damage control approach includes an adaptive LQR controller, a structural health monitoring module, and a state observer, all of them updated based on the identification module output.

Structures are often submitted to repetitive disturbances, with some critical regions more affected than others. The repeating cycle eventually leads to damage in these regions due to a fatigue process, which demands an SHM technique to be adopted to prevent failure. The proposed DTAC methodology retards damage occurrence and limits its propagation in these critical regions, combining preventive active control and evolving damage active control strategies to design a nonreconfigurable controller. Fig. 1 illustrates the adopted strategy framework. Piezoelectric transducers constitute the sensor and actuator network in the critical regions. Piezoelectric patches are widely used in smart structures for vibration control, due to their reversible property, which permits their use as sensors and/or actuators. Simulations of damage situations provide damage impact on modes, based on preliminary knowledge from structure analysis, fatigue tests, and maintenance history. Considering the respective impact assessment on each critical mode, the modal H_∞ controller is designed to create an energy distribution to mitigate damage effects.
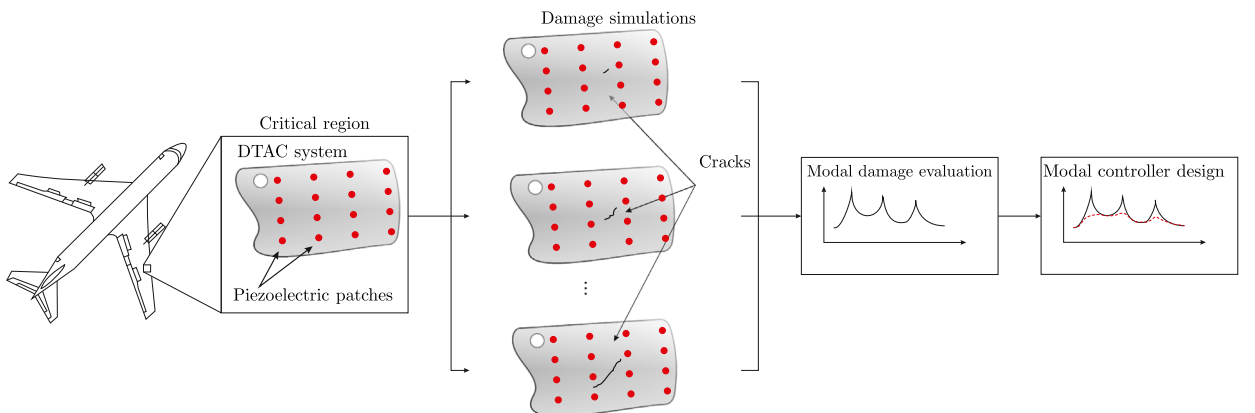

Fig. 1. Adopted DTAC strategy.

3. State-space modal representation

This section presents a brief overview of the modal state-space representation to describe a generic flexible structure, for the sake of completeness. This overview begins with a second-order matrix differential equation, commonly used to represent structural dynamics by means of FE models. Then, the state-space model is defined from this differential equation, using a specific state-vector definition. To conclude, the transformation matrices to obtain different modal canonical representations are presented.

A generic flexible structure can be modeled by the following second-order differential pair of equations:

$$\mathbf{M}\ddot{\mathbf{p}}(t) + \mathbf{D}\dot{\mathbf{p}}(t) + \mathbf{K}\mathbf{p}(t) = \mathbf{B_w}\mathbf{w}(t) + \mathbf{B_u}\mathbf{u}(t) \tag{1}$$

$$\mathbf{y}(t) = \mathbf{C_d}\mathbf{p}(t) + \mathbf{C_v}\dot{\mathbf{p}}(t) + \mathbf{C_w}\mathbf{w}(t) + \mathbf{C_u}\mathbf{u}(t), \tag{2}$$

in which $\mathbf{p}(t)$ denotes the displacements, $\mathbf{M}$ is the mass matrix, $\mathbf{D}$ is the damping matrix, $\mathbf{K}$ is the stiffness matrix, $\mathbf{B_w}$ and $\mathbf{B_u}$ are the respective input matrices, where $\mathbf{w}(t)$ are the disturbance forces acting on the structure and $\mathbf{u}(t)$ are the control forces, $\mathbf{y}(t)$ are the measured output signals modeled through the output matrices $\mathbf{C_d}$, $\mathbf{C_v}$, $\mathbf{C_w}$, and $\mathbf{C_u}$. In general, FE models generate high order models, which need to be reduced to represent the interest bandwidth for the controller operation. A simple truncation procedure, respecting the modes that present a significant energy level, is often enough to achieve good results. Therefore, the model reduction can be obtained using only a specific number of selected modes. The corresponding modal matrix is defined in the following equation, assuming m as the adopted number of modes:

$$\boldsymbol{\Phi} = \begin{bmatrix} \phi_1 & \phi_2 & \cdots & \phi_m \end{bmatrix}.$$

A transformation into modal coordinates is obtained using $\mathbf{p}(t) = \boldsymbol{\Phi}\mathbf{q}(t)$. Pre-multiplying Eq. (1) by $\boldsymbol{\Phi}^T$ gives:

$$\boldsymbol{\Phi}^T\mathbf{M}\boldsymbol{\Phi}\ddot{\mathbf{q}}(t) + \boldsymbol{\Phi}^T\mathbf{D}\boldsymbol{\Phi}\dot{\mathbf{q}}(t) + \boldsymbol{\Phi}^T\mathbf{K}\boldsymbol{\Phi}\mathbf{q}(t) = \boldsymbol{\Phi}^T\mathbf{B_w}\mathbf{w}(t) + \boldsymbol{\Phi}^T\mathbf{B_u}\mathbf{u}(t)$$

$$\mathbf{y}(t) = \mathbf{C_d}\boldsymbol{\Phi}\mathbf{q}(t) + \mathbf{C_v}\boldsymbol{\Phi}\dot{\mathbf{q}}(t) + \mathbf{C_w}\mathbf{w}(t) + \mathbf{C_u}\mathbf{u}(t),$$

which may be written as:

$$\mathbf{M_m}\ddot{\mathbf{q}}(t) + \mathbf{D_m}\dot{\mathbf{q}}(t) + \mathbf{K_m}\mathbf{q}(t) = \mathbf{B_{w_m}}\mathbf{w}(t) + \mathbf{B_{u_m}}\mathbf{u}(t) \tag{3}$$

$$\mathbf{y}(t) = \mathbf{C_{d_m}}\mathbf{q}(t) + \mathbf{C_{v_m}}\dot{\mathbf{q}}(t) + \mathbf{C_w}\mathbf{w}(t) + \mathbf{C_u}\mathbf{u}(t), \tag{4}$$

where $\mathbf{M_m} = \boldsymbol{\Phi}^T\mathbf{M}\boldsymbol{\Phi}$, $\mathbf{D_m} = \boldsymbol{\Phi}^T\mathbf{D}\boldsymbol{\Phi}$, $\mathbf{K_m} = \boldsymbol{\Phi}^T\mathbf{K}\boldsymbol{\Phi}$, $\mathbf{B_{w_m}} = \boldsymbol{\Phi}^T\mathbf{B_w}$, $\mathbf{B_{u_m}} = \boldsymbol{\Phi}^T\mathbf{B_u}$, $\mathbf{C_{d_m}} = \mathbf{C_d}\boldsymbol{\Phi}$, and $\mathbf{C_{v_m}} = \mathbf{C_v}\boldsymbol{\Phi}$. Matrices $\mathbf{M_m}$ and $\mathbf{K_m}$ are diagonal while $\mathbf{D_m}$ is not necessarily diagonal. For analytical convenience, the damping matrix is commonly considered as a linear combination of the stiffness and the mass matrices, $\mathbf{D} = \alpha\mathbf{M} + \beta\mathbf{K}$ for $\alpha, \beta \geq 0$ [36]. This is a reasonable and usual assumption, considering that flexible structures have small damping factors.

Assuming that the matrix $\mathbf{M_m}$ is nonsingular, Eq. (3) can be written as:

$$\ddot{\mathbf{q}}(t) + \mathbf{M_m^{-1}}\mathbf{D_m}\dot{\mathbf{q}}(t) + \mathbf{M_m^{-1}}\mathbf{K_m}\mathbf{q}(t) = \mathbf{M_m^{-1}}\mathbf{B_{w_m}}\mathbf{w}(t) + \mathbf{M_m^{-1}}\mathbf{B_{u_m}}\mathbf{u}(t). \tag{5}$$

Adopting the state-vector definition as:

$$\mathbf{x}(t) = \begin{bmatrix} \mathbf{x}_1(t) \\ \mathbf{x}_2(t) \end{bmatrix} = \begin{bmatrix} \mathbf{q}(t) \\ \dot{\mathbf{q}}(t) \end{bmatrix},$$

Eqs. (4) and (5) can be transformed into:

$$\dot{\mathbf{x}}_1(t) = \mathbf{x}_2(t)$$

$$\dot{\mathbf{x}}_2(t) = -\mathbf{M_m^{-1}}\mathbf{K_m}\mathbf{x}_1(t) - \mathbf{M_m^{-1}}\mathbf{D_m}\mathbf{x}_2(t) + \mathbf{M_m^{-1}}\mathbf{B_{w_m}}\mathbf{w}(t) + \mathbf{M_m^{-1}}\mathbf{B_{u_m}}\mathbf{u}(t)$$

$$\mathbf{y}(t) = \mathbf{C_{d_m}}\mathbf{x}_1(t) + \mathbf{C_{v_m}}\mathbf{x}_2(t) + \mathbf{C_w}\mathbf{w}(t) + \mathbf{C_u}\mathbf{u}(t),$$

leading to the following state-space representation:

$$\dot{\mathbf{x}}(t) = \mathbf{A}\mathbf{x}(t) + \mathbf{B}_1\mathbf{w}(t) + \mathbf{B}_2\mathbf{u}(t)$$

$$\mathbf{y}(t) = \mathbf{C}_2\mathbf{x}(t) + \mathbf{D}_{21}\mathbf{w}(t) + \mathbf{D}_{22}\mathbf{u}(t),$$

in which $\mathbf{C}_2 = [\mathbf{C_{d_m}}\ \mathbf{C_{v_m}}]$, $\mathbf{D}_{21} = \mathbf{C_w}$, and $\mathbf{D}_{22} = \mathbf{C_u}$. The matrices $\mathbf{A}$, $\mathbf{B}_1$, and $\mathbf{B}_2$ are obtained as:

$$\mathbf{A} = \begin{bmatrix} \mathbf{0} & \mathbf{I} \\ -\mathbf{M_m^{-1}}\mathbf{K_m} & -\mathbf{M_m^{-1}}\mathbf{D_m} \end{bmatrix}, \quad \mathbf{B}_1 = \begin{bmatrix} \mathbf{0} \\ \mathbf{M_m^{-1}}\mathbf{B_{w_m}} \end{bmatrix}, \quad \text{and} \quad \mathbf{B}_2 = \begin{bmatrix} \mathbf{0} \\ \mathbf{M_m^{-1}}\mathbf{B_{u_m}} \end{bmatrix}.$$

Finally, this model can be written into modal canonical representations using transformation matrices [36]. For the purpose of the paper approach, the following state-space model structure is adopted:

$$\bar{\mathbf{A}} = \begin{bmatrix} \mathbf{A_1} & \mathbf{0} & \cdots & \mathbf{0} \\ \mathbf{0} & \mathbf{A_2} & \cdots & \mathbf{0} \\ \vdots & \vdots & \ddots & \vdots \\ \mathbf{0} & \mathbf{0} & \cdots & \mathbf{A_m} \end{bmatrix}, \quad \bar{\mathbf{B}}_1 = \begin{bmatrix} \mathbf{B_{11}} \\ \mathbf{B_{12}} \\ \vdots \\ \mathbf{B_{1m}} \end{bmatrix}, \quad \bar{\mathbf{B}}_2 = \begin{bmatrix} \mathbf{B_{21}} \\ \mathbf{B_{22}} \\ \vdots \\ \mathbf{B_{2m}} \end{bmatrix}, \quad \text{and} \quad \bar{\mathbf{C}}_2 = \begin{bmatrix} \mathbf{C_{21}^T} \\ \mathbf{C_{22}^T} \\ \vdots \\ \mathbf{C_{2m}^T} \end{bmatrix}^T,$$

where it is possible to see that the system matrix has a block diagonal structure where each $\mathbf{A}_i$ is a 2×2 matrix for $i = 1, \ldots, m$, therefore isolating each mode.

4. Modal robust control

According to the optimal controller design framework, a performance indicator is introduced as an output vector $\mathbf{z}(t)$, leading to the following state-space equations:

$$\dot{\mathbf{x}}(t) = \bar{\mathbf{A}}\bar{\mathbf{x}}(t) + \bar{\mathbf{B}}_1\mathbf{w}(t) + \bar{\mathbf{B}}_2\mathbf{u}(t)$$
$$\mathbf{z}(t) = \mathbf{C_1}\bar{\mathbf{x}}(t) + \mathbf{D_{11}}\mathbf{w}(t) + \mathbf{D_{12}}\mathbf{u}(t)$$
$$\mathbf{y}(t) = \bar{\mathbf{C}}_2\bar{\mathbf{x}}(t) + \mathbf{D_{21}}\mathbf{w}(t) + \mathbf{D_{22}}\mathbf{u}(t), \tag{6}$$

in which the matrices $\mathbf{C_1}$, $\mathbf{D_{11}}$, and $\mathbf{D_{12}}$ are chosen to define the desired performance vector. To be consistent with the adopted modal system matrix, this vector can be written in terms of a sum of modal performances as $\mathbf{z}(t) = \sum_{i=1}^{m} \mathbf{z}_i(t)$, in which $\mathbf{z}_i(t)$ represents the performance signals relative to mode i. A spectral composition of the disturbance vector $\mathbf{w}(t)$ is also adopted, without loss of generality, as m contiguous frequency bands, such that $\mathbf{w}(t) = \sum_{i=1}^{m} \mathbf{w}_i(t)$, where each band is chosen in order to contain only one natural frequency.

Given a state-space controller K_c as:

$$\dot{\mathbf{x}}_c(t) = \mathbf{A}_c\mathbf{x}_c(t) + \mathbf{B}_c\mathbf{y}(t)$$
$$\mathbf{u}(t) = \mathbf{C}_c\mathbf{x}_c(t) + \mathbf{D}_c\mathbf{y}(t), \tag{7}$$

the regular H_∞ control problem comes down to obtain the controller matrices by the minimization of the following objective function:

$$J_\infty = \frac{\int_0^\infty \mathbf{z}^T(t)\mathbf{z}(t)dt}{\int_0^\infty \mathbf{w}^T(t)\mathbf{w}(t)dt}. \tag{8}$$

Similarly, given the controller represented by Eq. (7), the modal H_∞ control problem aims to find a controller whose closed-loop system satisfies the new objective modal function [33]:

$$\underbrace{\inf}_{K_c \in V} \underbrace{\sup}_{\mathbf{w} \neq 0, \, \mathbf{w} \in \mathcal{L}_2[0, \infty[} J_m < \gamma^2,$$

in which V represents the set of all controllers that stabilizes the plant and:

$$J_m = \frac{\sum_{i=1}^{m} \int_0^\infty \mathbf{z}_i^T(t)\mathbf{Q}_i\mathbf{z}_i(t)dt}{\sum_{i=1}^{m} \int_0^\infty \mathbf{w}_i^T(t)\mathbf{w}_i(t)dt}, \tag{9}$$

where $\mathbf{Q}_i = \mathbf{Q}_i^T > 0$ is the weighing matrix relative to mode i. The purpose of the diagonal matrix $\mathbf{Q}_i$ is to describe the desired attenuation rate of mode i, whose results lead to the searched mode selectivity.

The modal problem can then be transformed into an equivalent H_∞ problem using the following system [33]:

$$\dot{\bar{\mathbf{x}}}(t) = \bar{\mathbf{A}}\bar{\mathbf{x}}(t) + \bar{\mathbf{B}}_1\mathbf{w}(t) + \bar{\mathbf{B}}_2\mathbf{u}(t)$$
$$\mathbf{z_m}(t) = \Gamma\bar{\mathbf{x}}(t) + \Theta\mathbf{w}(t) + \Lambda\mathbf{u}(t)$$
$$\mathbf{y} \ \ (t) = \bar{\mathbf{C}}_2\bar{\mathbf{x}}(t) + \mathbf{D_{21}}\mathbf{w}(t) + \mathbf{D_{22}}\mathbf{u}(t),$$

with $\Gamma = [\mathbf{Q}_1^{\frac{1}{2}}\mathbf{C_{1_1}} \ \mathbf{Q}_2^{\frac{1}{2}}\mathbf{C_{1_2}} \ \cdots \ \mathbf{Q_m}^{\frac{1}{2}}\mathbf{C_{1m}}]$, $\Theta = (\mathbf{Q}_1^{\frac{1}{2}}\mathbf{D_{11_1}} + \cdots + \mathbf{Q_m}^{\frac{1}{2}}\mathbf{D_{11m}})$, $\Lambda = (\mathbf{Q}_1^{\frac{1}{2}}\mathbf{D_{12_1}} + \cdots + \mathbf{Q_m}^{\frac{1}{2}}\mathbf{D_{12m}})$, where $\mathbf{C_{1_i}}$, $\mathbf{D_{11_i}}$, and $\mathbf{D_{12_i}}$ are the components of $\mathbf{C_1}$, $\mathbf{D_{11}}$, and $\mathbf{D_{12}}$ relative to mode i. Thus, Eq. (9) may be rewritten as:

$$J_m = \frac{\int_0^\infty \mathbf{z_m}^T(t)\mathbf{z}_m(t)dt}{\int_0^\infty \mathbf{w}^T(t)\mathbf{w}(t)dt}, \tag{10}$$

which is similar to the regular H_∞ objective function, meaning that known tools may be applied to solve this problem.

Fig. 2 represents a regular H_∞ framework [36–38] that is adopted to solve the modal robust problem, as seen above,
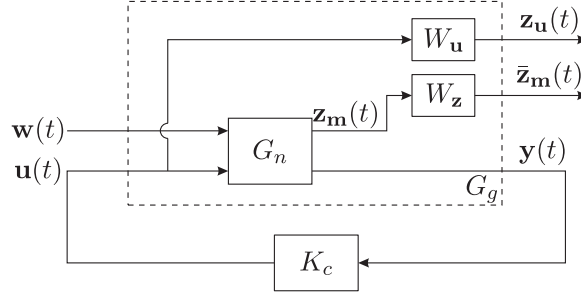
Fig. 2. Block diagram of the H_∞ control problem.

however including frequency band restrictions to avoid the spillover. This is done through the weighing filters $W_\mathbf{u}$ and $W_\mathbf{z}$ whose outputs are, respectively, $\mathbf{z}_u(t)$ and $\bar{\mathbf{z}}_\mathbf{m}(t)$. The nominal plant G_n is obtained from the modal reduced model, G_g is the generalized plant including the filters, and the respective nominal controller is K_c.

The weighing filter design corresponds to a process that usually involves many iterations to achieve fine tuning. $W_\mathbf{z}(s)$ is chosen as a low-pass filter and $W_\mathbf{u}(s)$ is designed as a high-pass filter. The following representations for these filters are adopted as [38]:

$$
W_\mathbf{z}(s) = \left(\frac{\frac{s}{\sqrt[k]{M}} + \omega_c}{s + \omega_c \sqrt[k]{\varepsilon}} \right)^k \quad \text{and} \quad W_\mathbf{u}(s) = \left(\frac{s + \frac{\omega_c}{\sqrt[k]{M}}}{s\sqrt[k]{\varepsilon} + \omega_c} \right)^k,
$$

(11)

in which ω_c, k, ε, and M determine the transition frequency between rejection band and pass band, the filter order, the gain at pass band, and the gain at rejection band, respectively.

The transfer matrix between the performance output $\hat{\mathbf{z}}_\mathbf{m}(t) = \left[\bar{\mathbf{z}}_\mathbf{m}^T(t) \ \mathbf{z}_\mathbf{u}^T(t) \right]^T$ and the disturbance $\mathbf{w}(t)$ is defined as $T_{\hat{\mathbf{z}}_\mathbf{m}\mathbf{w}}$. The objective function, given in Eq. (10), is the modal H_∞ norm, which is extended to $\| T_{\hat{\mathbf{z}}_\mathbf{m}\mathbf{w}} \|_\infty$. A suboptimal approach is adopted to solve the respective H_∞ control problem, based on successive iterations to find the controller. Therefore, the robust modal controller design can be formulated as a convex optimization problem, adopting a well-known procedure presented in [37,39].

5. Determination of the modal weighing matrices

A subspace metric to quantify damage effects on structure modes is here proposed to enable the inclusion of damage as a controller design requirement. The regular approach for this metric is the assessment of the distance between subspaces representing a healthy and a damaged model, based on dynamic response changes as damage indicators. For instance, Zheng and Mita [40] applied a subspace metric to monitor the structural health of a simulated structure with five storeys subject to ambient and seismic excitations. Genari et al. [41] investigated the metric for detection, severity analysis, and location of damage experimentally, considering a medium frequency range. However, these metric applications do not provide information about damage effects on each mode. To overcome this limitation, the subspace metric is here modified to provide modal damage effects, based on the adopted state-space modal model. Using this data, the modal weighing matrices are then estimated in order to compensate each affected mode.

5.1. Modal damage metric

The infinite observability matrix for the flexible structure M described by Eq. (6) is defined as:

$$
O_\infty(M) = \left[(\bar{\mathbf{C}}_\mathbf{2})^T \ (\bar{\mathbf{C}}_\mathbf{2}\bar{\mathbf{A}})^T \ (\bar{\mathbf{C}}_\mathbf{2}\bar{\mathbf{A}}^\mathbf{2})^T \ \cdots \right]^T.
$$

Assuming that $M^{(1)}$ and $M^{(2)}$ are two stable models with order $2m$, the respective observability matrices are $O_\infty(M^{(1)})$ and $O_\infty(M^{(2)})$. The distance between $M^{(1)}$ and $M^{(2)}$ can be calculated in terms of the principal angles between the subspace ranges $O_\infty(M^{(1)})$ and $O_\infty(M^{(2)})$ (see [42] for details). Thus, the distance between $M^{(1)}$ and $M^{(2)}$ is given by:

$$
\Delta(M^{(1)}, M^{(2)})^2 = \log \left(\prod_{l=1}^{2m} \frac{1}{\cos^2 \theta_l} \right),
$$

(12)

in which θ_l is the lth principal angle between the subspace ranges $O_\infty(M^{(1)})$ and $O_\infty(M^{(2)})$.

The distance computed by Eq. (12) is a scalar indicator, which does not take into account modal effects. To get a modal indicator, the metric is here modified to calculate damage impact on each vibration mode. Decomposing M into m modal

subsystems, the infinite observability matrix of a modal subsystem M_i is defined as:

$$O_\infty(M_i) = \left[(\bar{\mathbf{C}}_{\mathbf{2_i}})^T \ (\bar{\mathbf{C}}_{\mathbf{2_i}}\bar{\mathbf{A}}_{\mathbf{i}})^T \ (\bar{\mathbf{C}}_{\mathbf{2_i}}\bar{\mathbf{A}}_{\mathbf{i}}^2)^T \ \cdots \right]^T,$$

(13)

where $\bar{\mathbf{C}}_{\mathbf{2_i}}$ and $\bar{\mathbf{A}}_i$, respectively, represent the elements of $\bar{\mathbf{C}}_{\mathbf{2}}$ and $\bar{\mathbf{A}}$ relative to mode i. The distance between $M_i^{(1)}$ and $M_i^{(2)}$ for mode i is then proposed as:

$$\Delta_i(M_i^{(1)}, M_i^{(2)})^2 = \log\left(\prod_{j=1}^{2} \frac{1}{\cos^2 \theta_j} \right).$$

(14)

5.2. Modal weighing matrices

Considering the above definition of modal distances, this subsection presents an original approach that allows inserting damage information into the modal H_∞ controller design, using the modal weighing matrices. Structural damage may lead to modal vibration increase or reduction, depending on several factors. The modal distance technique permits to evaluate damage effects on the modes, but it is not able to distinguish if its vibration amplitude is increasing or reducing.

To overcome this limitation, the proposed method assesses the effect of a regular H_∞ controller on the *healthy* structure. The idea is to use, for each mode of the healthy structure, its closed-loop attenuation and the respective peak values. Associating these two values to the modal damage effects on the structure, i.e., the modal distances between the open-loop response of the healthy and of the damaged structure, it gives an indication of the amplitude variation and also of the respective importance of each mode. With these data, it is possible to obtain a relation to provide the modal damage amplitude weighing that can be used to design the damage-tolerant controller.

Considering p different performance signals, Fig. 3 shows the open-loop amplitude frequency response of the healthy structure and also the closed-loop response using the regular H_∞ controller, between the performance signal $\mathbf{z}_l(t)$ for $l = 1, \ldots, p$ and the disturbance $\mathbf{w}(t)$. The following indicator balances the vibration reduction achieved by the controller and the relative effect of the damage for each mode:

$$\bar{\mathbf{q}}_l = \left[\left(\frac{\alpha_{l1}\Delta_1}{\phi_{l1}} \right) \left(\frac{\alpha_{l2}\Delta_2}{\phi_{l2}} \right) \cdots \left(\frac{\alpha_{lm}\Delta_m}{\phi_{lm}} \right) \right],$$

(15)

in which Δ_i is the calculated modal distance, α_{li} is the modal peak amplitude of the controlled structure and ϕ_{li} is the modal peak reduction, for $i = 1, \ldots, m$.

Notice that each factor in Eq. (15) shall correspond to an element of the modal weighing matrices. However, considering the relative values of these parameters, it is possible to have very small or very large numbers. To limit these numbers, it is convenient to establish an amplitude transformation, taking into account the minimum and the maximum values of the vector given by Eq. (15). Attributing two new values for these numbers, the adopted transformation is the line equation formed by these two points in a plane. The new values must conduct the parameters to a reasonable range, chosen based on practical aspects, e.g., maximum output voltage. The new consistent vector is now:

$$\mathbf{q}_l = \left[\beta_{l1} \ \beta_{l2} \ \cdots \ \beta_{lm} \right],$$

(16)

which leads to the following modal weighing matrices:

$$\mathbf{Q}_{\mathbf{1}}^{\frac{1}{2}} = \begin{bmatrix} \beta_{11} & 0 & 0 & 0 \\ 0 & \beta_{21} & 0 & 0 \\ \vdots & \vdots & \ddots & \vdots \\ 0 & 0 & 0 & \beta_{p1} \end{bmatrix}, \ \ldots, \ \mathbf{Q}_{\mathbf{m}}^{\frac{1}{2}} = \begin{bmatrix} \beta_{1m} & 0 & 0 & 0 \\ 0 & \beta_{2m} & 0 & 0 \\ \vdots & \vdots & \ddots & \vdots \\ 0 & 0 & 0 & \beta_{pm} \end{bmatrix},$$
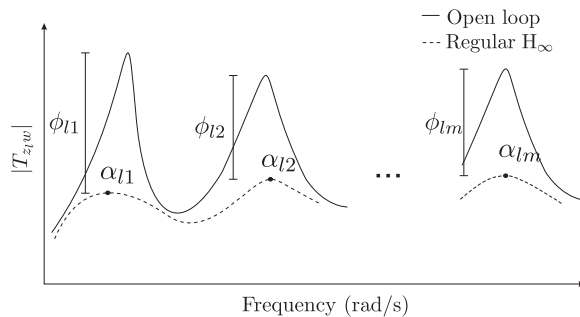
(17)

Fig. 3. $T_{z_l|\mathbf{w}}$ attenuation and peak values.

where the weighing matrices are responsible for distributing the control signal energy among the modes, conducting to modal selectivity.

The following algorithm summarizes the steps to design the damage-tolerant controller:

Algorithm 1. Damage-tolerant controller.

1: Determine the modal state-space model of the healthy plant (Eq. (6)) and the respective observability matrices (Eq. (13));
2: Estimate the observability matrices for the damaged plant and calculate the subspace angles for each mode;
3: Design the regular H_∞ controller by solving the respective optimization problem (Eq. (8));
4: Compute the subspace distances for each mode between the healthy and damaged models (Eq. (14));
5: Compute the raw indicator of each mode considering the amplitude variation due to damage (Eq. (15)) and transform them into consistent values (Eq. (16));
6: Build the modal weighing matrices (Eq. (17));
7: Design the modal H_∞ controller by solving the respective optimization problem (Eq. (10)).

6. Simulated results

This section presents details of the healthy and the damaged structure, using FE models. In the sequence, a regular H_∞ controller (RC) and a modal H_∞ controller (MC) are designed to reduce structural vibration caused by disturbance. Recall that only the MC design uses damage information through the weighing matrices, as already described. Next, simulated controller performances are analyzed and compared.

Considering the classical approach of linear constitutive relations for materials with small mechanical and electrical perturbations [43,44], the proposed method is general and does not rely on a particular shape or boundary conditions of the controlled structure. The only requirement is that the structure can be modeled by means of a theory that leads to Eqs. (1) and (2). Using a dedicated software, the FE method gives a general frame to get such equations and models any linear physical structure. As the accuracy is governed by the quality of the discretization, accurate models can lead to a high number of degrees of freedom.

The example of an active aluminum structure chosen to demonstrate the application of the proposed modal H_∞ technique is shown in Fig. 4a, according to the guidelines presented in Fig. 4b. This structure is a 600 mm × 30 mm uniform aluminum plate, equipped with four pairs of piezoelectric ceramic elements bonded on its upper and lower faces, as shown in Fig. 5. The respective thicknesses are 3.2 mm for the plate and 0.5 mm for each piezoelectric ceramic element. The control signal $u(t)$ and the disturbance $w(t)$ are applied to the actuators while the sensors generate, respectively, the signals $y_1(t)$ and $y_2(t)$. The adopted structure is simulated using a dedicated FE software, named PLQP and developed at the PIMM
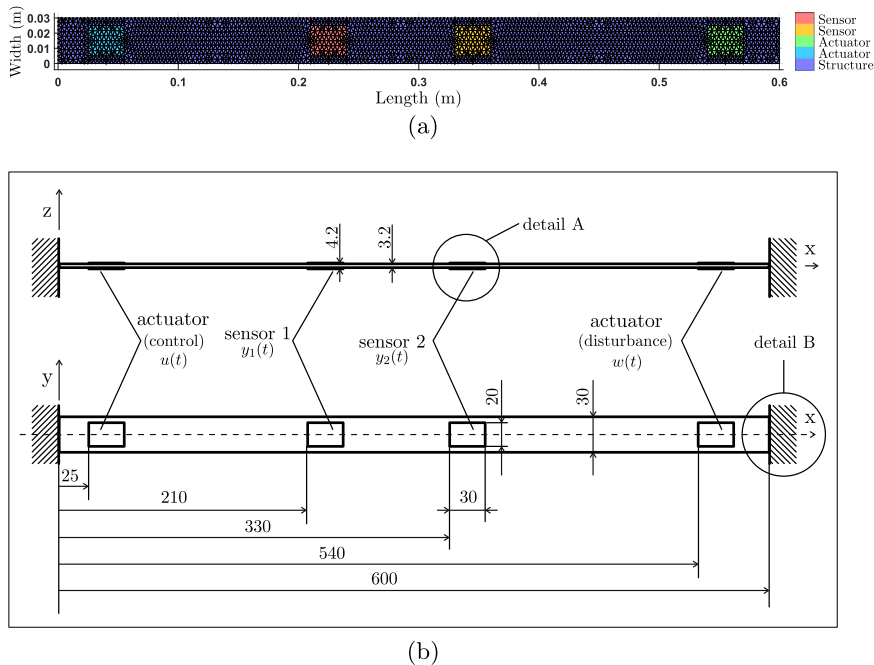
Fig. 4. The adopted aluminum structure with active elements: (a) flexible structure modeled by the PLQP software and (b) schematic diagram (scaled in mm).
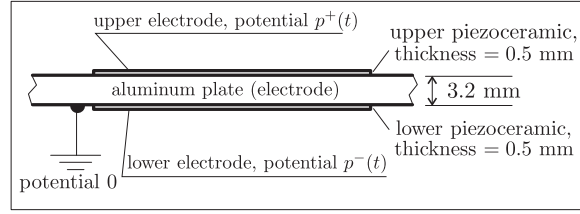
Fig. 5. Detail A of Fig. 4(b): configuration of each couple of piezoceramic elements.

Laboratory of Arts et Métiers ParisTech, to test control strategies on plates. The FE model mesh contains 2186 nodes and 3939 discrete Kirchhoff triangular plate elements [43], considering 472 elements to model the four areas where the piezoelectric transducers are placed. Three degrees of freedom (DOFs), a translation degree and two rotation degrees, are used to describe the transverse motion (motion along z) of each node of the plate. Thus, it leads to 6558 mechanical DOFs and four electrical DOFs, which describe the electric voltage $p_j(t)$ applied to each external electrode of ceramics couples, for $j = 1, ..., 4$. The electric potential is constant and orthogonal to the plane (x,y) in each piezoelectric layer. These ceramics have an isotropic behavior in the plane (x,y), the direction of polarization is z, and they are covered with electrodes. The aluminum core imposes the same potential of reference (0) to the electrodes at $z = \pm 1.6$ mm and the electric connections imply equal potentials $p_j^+(t) = p_j^-(t) = p_j(t)$ on the external electrodes ($z = \pm 1.85$ mm). Material properties of the structure and of the piezoelectric elements are given in Appendix A.

The nominal plant model used to design the controllers is reduced to four modes. Another model with ten modes, referred here as the complete model, is adopted to analyze the controller performance, in order to verify that the controller is effectively avoiding spillover. Comparison of the open-loop transfer functions for both models is presented in Fig. 6. The respective vibration modes and natural frequencies are presented in Table 1.

6.1. Damage simulation

When the perfect boundary conditions at $x=0$ and $x=600$ mm are considered, the aspect ratio allows to model this active structure as a clamped–clamped beam if the model aims to represent only the first modes of vibration. However, due to the consideration of a damaged clamping at $x=600$ mm, this assumption cannot be done and the structure is modeled as a Kirchhoff plate. The damage is simulated by a partial clamping at $x=600$ mm as shown in Fig. 7, representing a common damage in clamped structures. The length h of the free boundary governs the severity of this damage. It can be interpreted as the model of a crack of length h in the linking of the beam to the rigid frame. Damage severity is modified considering three different crack lengths:

- No damage: $h=0$.
- Damage 1: $h=10$ mm.
- Damage 2: $h=15$ mm.
- Damage 3: $h=20$ mm.
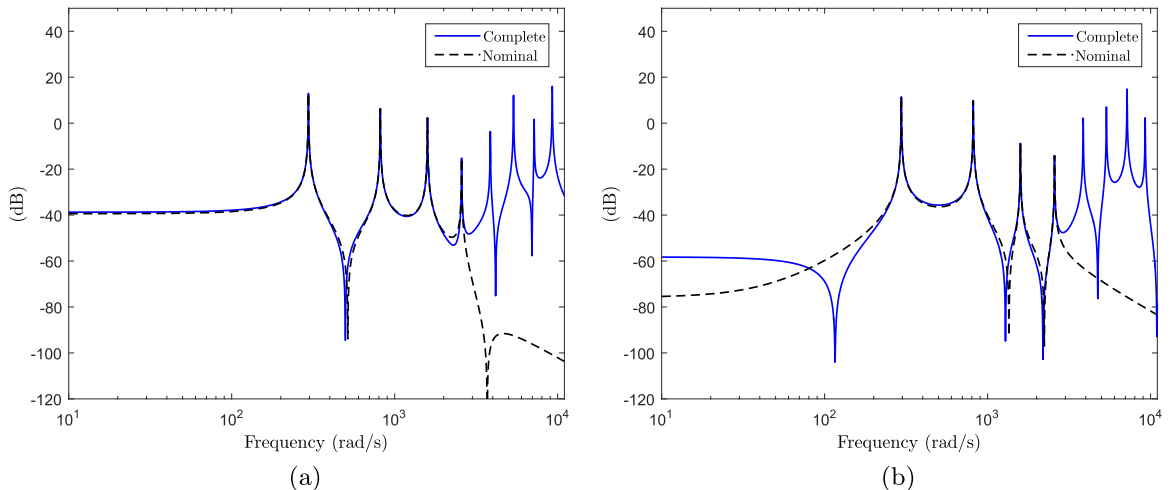
Fig. 6. Transfer function comparison between the complete and the nominal models: (a) $T_{y_1 w}$ and (b) $T_{y_2 w}$.

Table 1
First natural frequencies of the healthy structure.

| Mode	Frequency (rad/s)	Deformation	Mode	Frequency (rad/s)	Deformation
1	295.69	Bending	6	3861.10	Bending
2	816.72	Bending	7	5360.21	Bending
3	1590.10	Bending	8	7173.37	Bending
4	2574.19	Bending	9	7630.50	Torsion
5	3683.19	Torsion	10	9267.03	Bending
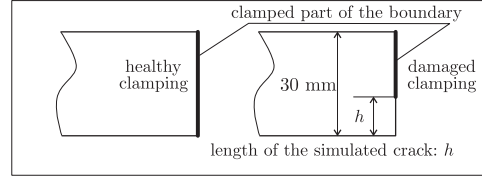
Fig. 7. Detail B of Fig. 4(b): modification of the boundary conditions to simulate a damage that models a crack.

Damage may induce different effects on each mode of vibration because the crack changes the boundary conditions, thus changing mode shapes. This can be seen in Fig. 8, which shows frequency responses from the healthy structure and the damaged structure for the damage 3. It is possible to notice natural frequency shifts in all modes and amplitude changes, higher in modes 3 and 4, which belong to the frequency range of interest. In mode 3, damage reduces the amplitude of vibrations while in mode 4 damage leads to a larger amplitude. Damage effects on the natural frequencies and modal amplitudes can be summarized in a single value for each vibration mode, using the modal damage metric. Fig. 9 presents the modal distances for the three damage cases, in which their increase with damage severity is easily seen. These results also show the proposed modal metric as a tool to assess damage severity.

6.2. Regular robust controller design

Regular robust controllers are commonly used to reduce vibration effects caused by disturbance. The regular controller is designed based on the nominal model of the healthy structure according to Eq. (6). The performance matrices are defined as $\mathbf{C_1} = \mathbf{C_2}$ and $\mathbf{D_{11}} = \mathbf{D_{12}} = [0\ 0]^T$. A chirp signal with band between 0 Hz and 500 Hz, duration of 20 s, and amplitude of 4 V is considered as the disturbance to examine the controller performance. The complete model is employed to close the loop. The spillover-avoiding capability is achieved using the weighing filters of Eq. (11), designed with the parameters present in Table 2.

Frequency and time responses for the open-loop and the closed-loop healthy structure are shown, respectively, in Figs. 10 and 11, which also show results for the modal controller presented in the next subsection. Fig. 10 presents frequency responses for the two performance outputs in the interest band. It can be seen the vibration reduction for all modes, with mode 4 presenting the lowest reduction. Table 3 details the vibration attenuation for each mode.
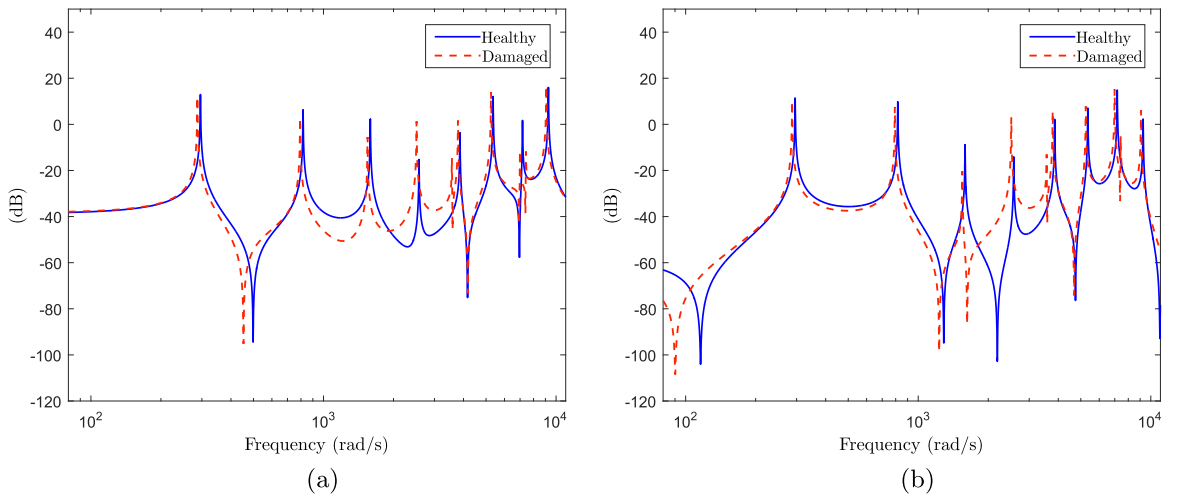
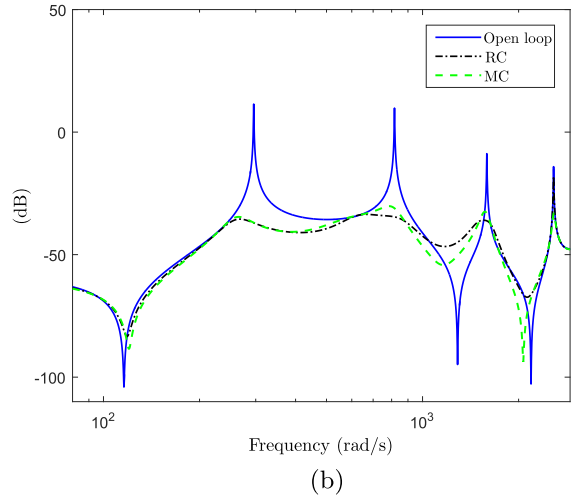**Fig. 8.** Frequency responses of the healthy and the damaged structures (damage 3): (a) $T_{y_1 w}$ and (b) $T_{y_2 w}$.
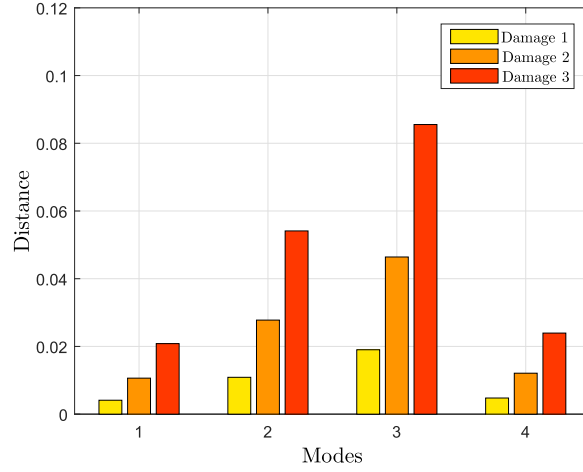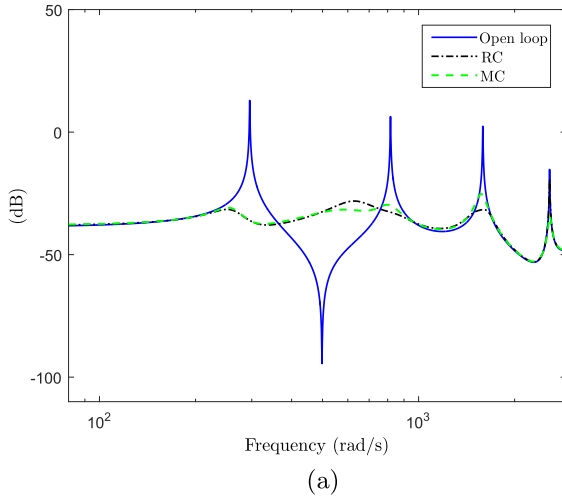
Fig. 9. Modal distance estimation.

| Weighing filters	ω_c	k	M	ε
W_u	2320	2	65	0.07
W_z	2320	1	65	0.07

Fig. 10. Frequency response comparison between the uncontrolled and controlled healthy structures: (a) $T_{z_1 w}$ and (b) $T_{z_2 w}$.

6.3. Modal robust controller design

The same controller structure is adopted for the modal robust controller design, adding the modal weighing matrices and the respective performance outputs. These matrices are determined based on the modal distances calculated between the open-loop healthy and damaged structures (damage 3), and using data contained in Table 3, according to Eq. (15). The minimum weighing value is 0.6 and the maximum value is 4.5. Based on these parameters, the following modal weighing matrices are calculated:

$$\mathbf{Q}_1^{\frac{1}{2}} = \begin{bmatrix} 0.6 & 0 \\ 0 & 0.6 \end{bmatrix}, \quad \mathbf{Q}_2^{\frac{1}{2}} = \begin{bmatrix} 0.7 & 0 \\ 0 & 0.6 \end{bmatrix}, \quad \mathbf{Q}_3^{\frac{1}{2}} = \begin{bmatrix} 0.7 & 0 \\ 0 & 0.7 \end{bmatrix}, \quad \text{and} \quad \mathbf{Q}_4^{\frac{1}{2}} = \begin{bmatrix} 4.5 & 0 \\ 0 & 4.5 \end{bmatrix}.$$
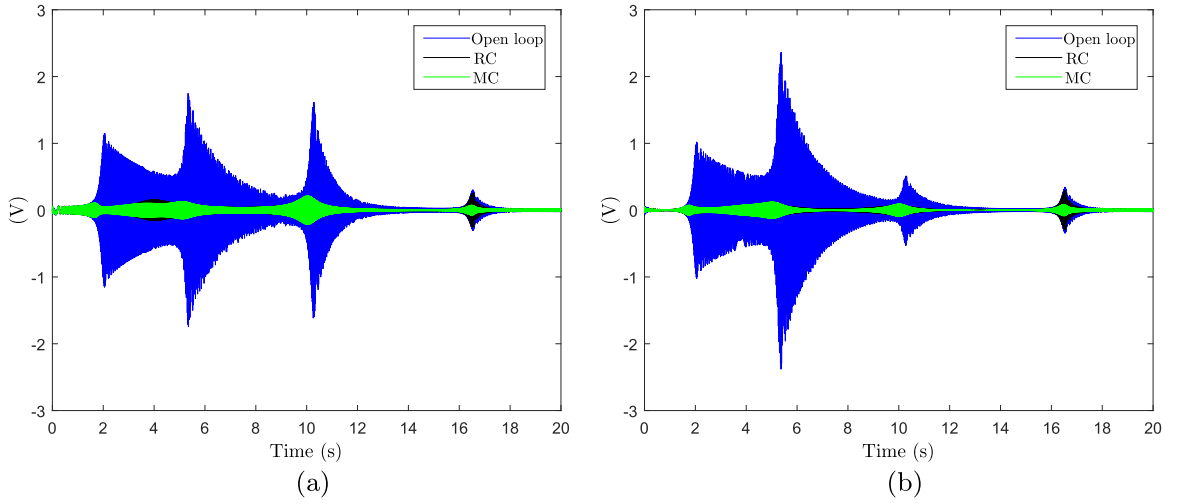
Fig. 11. Time domain responses of the uncontrolled and controlled healthy structures: (a) $y_1(t)$ and (b) $y_2(t)$.

Table 3
Healthy beam modal responses with the regular controller.

| Transfer function	Mode 1	Mode 2	Mode 3	Mode 4
Modal vibration reduction (dB; $|\phi|$)				
$T_{z_1 w}$	44.6; 169.82	34.0; 050.12	34.8; 55.95	4.2; 1.62
$T_{z_2 w}$	47.0; 223.87	43.4; 147.91	27.5; 23.71	4.2; 1.62
Controlled structure peaks (dB; $|T_{zw}|$)				
$T_{z_1 w}$	−31.5; 0.0266	−28.1; 0.0394	−31.6; 0.0266	−19.2; 0.1096
$T_{z_2 w}$	−35.5; 0.0168	−33.5; 0.0211	−35.9; 0.0160	−18.1; 0.1245
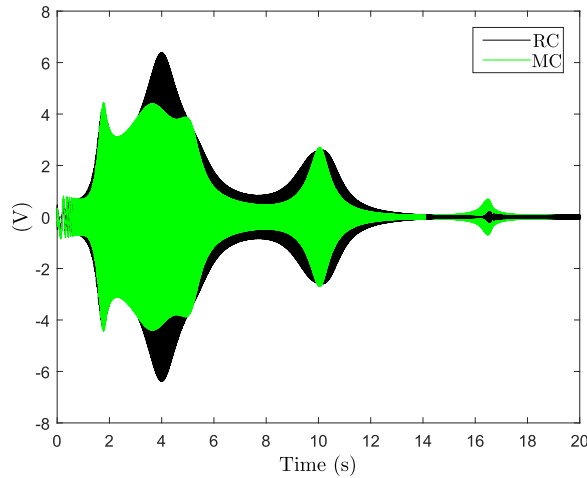
Fig. 12. Control signal comparison between the MC and the RC in the healthy structure.

These values imply that vibration mode 4 has the highest desired weighing factor. Notice that similar modal weighing matrices are obtained using the modal distances considering damage 1 or damage 2.

### 6.4. Healthy structure responses

The performance of both controllers is initially compared for the healthy structure. Frequency and time responses are presented in Figs. 10 and 11, respectively. It can be seen in both figures that, for mode 1, the controllers have similar performance. For modes 2 and 3, the RC performance is slightly better than the MC performance. These results are expected
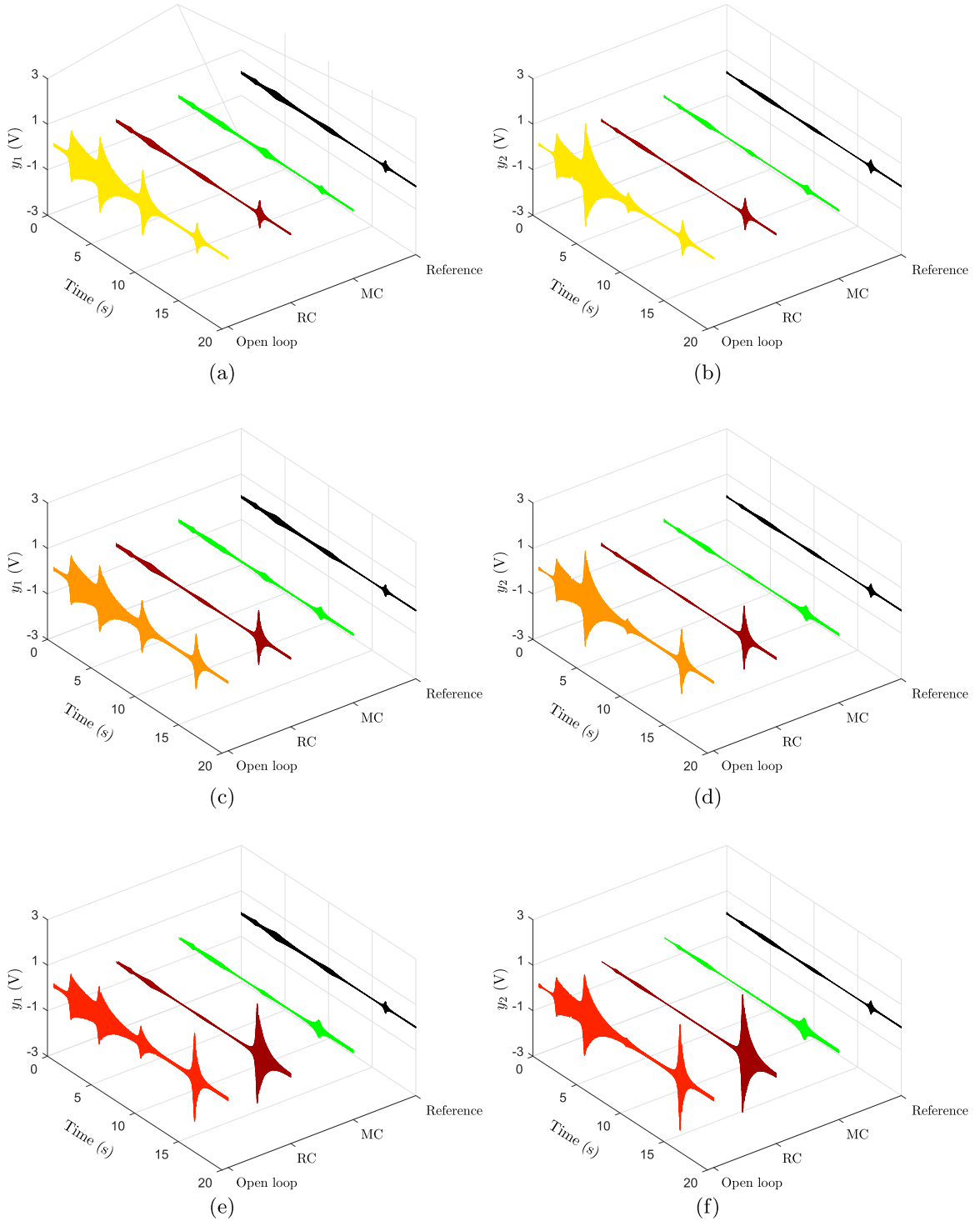
Fig. 13. Performance comparison of the controlled structure subjected to damage: (a) and (b) show $y_1(t)$ and $y_2(t)$ of the structure with damage 1; (c) and (d) show $y_1(t)$ and $y_2(t)$ of the structure with damage 2; (e) and (f) show $y_1(t)$ and $y_2(t)$ of the structure with damage 3.

because the MC has low weight in these modes. For mode 4, the MC performance is better than the RC, due to modal weighing increase in this mode. Fig. 11 also shows that there is no spillover excitation.

Fig. 12 permits to compare the RC and the MC control signals. It can be seen that the MC presents a better energy distribution, due to the relative specified modal weighing. Comparing with the RC, the MC control signal has its amplitude
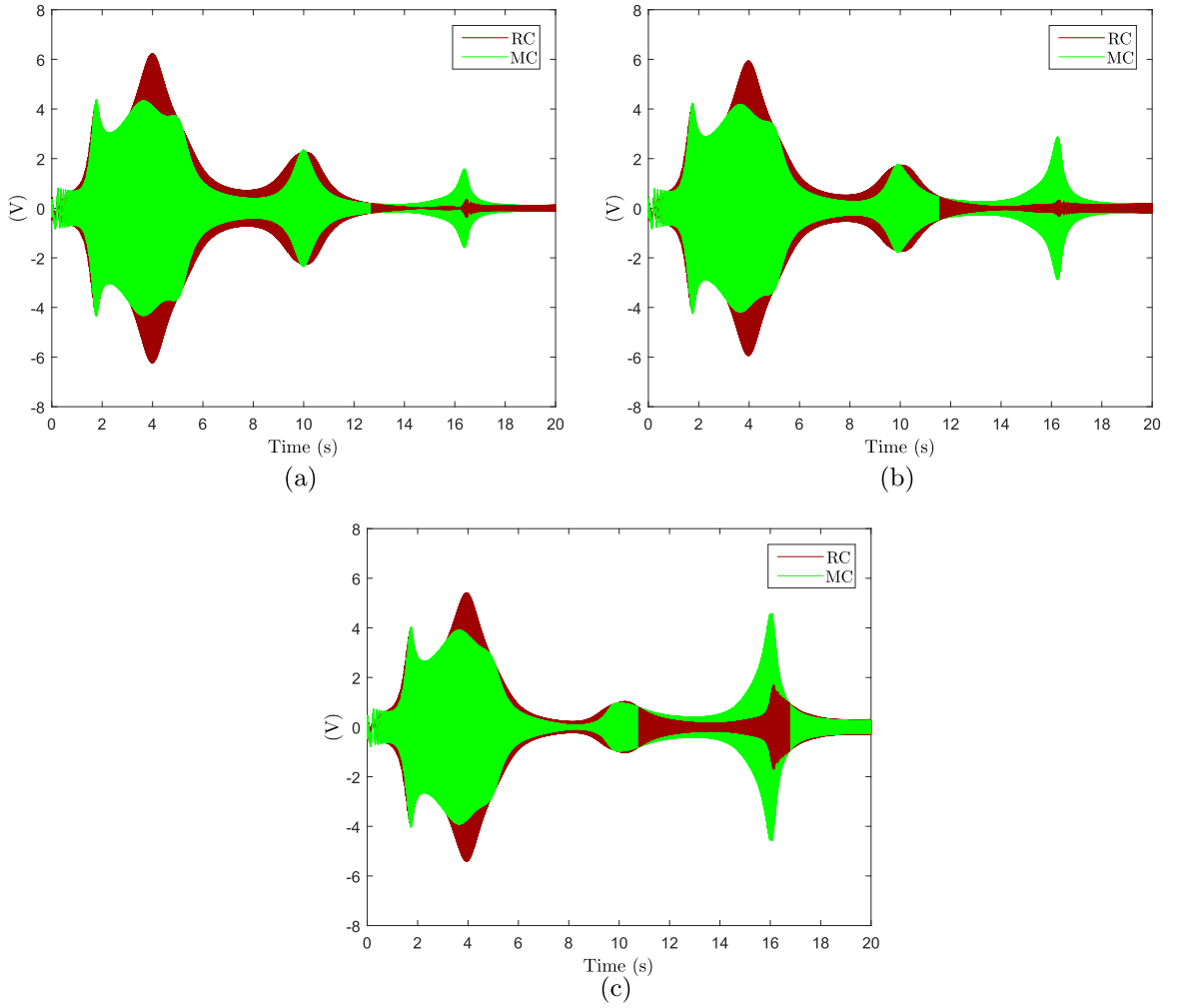
Fig. 14. Control signals of the structure subjected to damage: (a) damage 1, (b) damage 2, and (c) damage 3.

reduced in mode 2, is equivalent in modes 1 and 3, is amplified in mode 4, but its amplitude is low compared to mode 2. It can be affirmed that both controllers achieved satisfactory performance in the healthy structure vibration reduction.

6.5. Controller responses under damage

The adopted DTAC strategy aims to focus the control action on modes that are indeed suffering the worst damage consequences. For this purpose, the MC is designed to provide an appropriate energy distribution to mitigate damage effects, besides controlling the healthy structure, too. The MC is now examined under the three different damage conditions, representing a crack propagation, and is compared to the RC behavior. Time domain performance signals are presented in Fig. 13, in which the RC performance of the healthy structure is used as the reference.

It can be seen in Fig. 13 that modes 1, 2, and 3 are slightly affected by damage even for the higher severity case, with both controllers presenting similar performance, also close to the reference. Recall that for the uncontrolled structure this also occurs, but it is possible to notice that there are performance differences for mode 4, that increase significantly the vibration peak under RC, getting even higher than the open-loop vibration peaks. However, the MC maintains the mode 4 close to the reference and significantly smaller than the open-loop behavior.

Fig. 14 shows the control signal behavior for the two tested controllers. Comparing the control signal evolution among the three severity cases, their amplitudes decrease for both controllers for the three first modes, which are less affected by the damage, and increases for the fourth mode, as the severity progresses. However, it can be seen that the MC amplitude for mode 4 increases substantially, leading to the high attenuation seen in Fig. 13. The general result is an energy migration from the three first modes to the fourth, but this is more efficient with the MC.

It is also interesting to note that both controllers concentrate the energy for the attenuation in the first and second modes, which present the highest open-loop amplitude. The damage effect in the analyzed cases increases significantly the open-loop

vibrations of the fourth mode, which present a low amplitude compared to the first modes. Healthy mechanical structures usually behave as low-pass systems, but the damage renders the fourth mode higher than the other modes, as seen in Fig. 13e and f. The proposed method permits to foresee this effect and to design a controller that, being effective for the healthy structure, can present the damage-tolerant capability, which, as seen in the results, does not occur for a regular-designed controller.

7. Conclusions

An investigation of the damage-tolerant controller design based on a modal H_∞ norm was here conducted. The proposed methodology allows designing an effective control system for a healthy structure, which can also face damage effects. The adopted approach considers foreseen study results that can point the most stressed regions and, therefore, the most probable regions for a damage to occur. The same controller can achieve an adequate performance to the healthy and damaged structure, avoiding time delay due to a reconfigurable controller design process. As a consequence of these characteristics, the proposed method can also extend the operational life of the structures.

The damage controller achieves these goals by specifying modal weighing matrices to provide an adequate control signal energy distribution to mitigate damage effects. The adopted approach considers that structural damage impact is represented by a composition of damage effects on each mode, which may be quantified using a damage indicator based on a proposed modal distance. The modal damage indicator is used to build modal weighing matrices, used as a design requirement to provide an appropriate damage-tolerant controller. A transformation of the performance output vector of the regular H_∞ controller design includes these modal constraints, leading to an optimization problem that may be efficiently solved by known LMI methods.

The proposed methodology is validated using the FE modeling of a clamped–clamped beam, where controller response to three different damage severities was simulated. Performance results of the modal controller are shown to be more effective against damage impacts, compared to a regular H_∞ controller, due to the achieved modal selectivity. This feature is responsible for concentrating the control energy on the modes that are mostly affected by the damage. Moreover, the performance of the damage-tolerant controller is also adequate to the healthy structure, which yields the conclusion that the proposed modal approach can protect the structure as well, retarding damage occurrence.

Appendix A. Material properties

The material properties of the active aluminum structure are presented in Table A1. The piezoelectric element properties are shown in Table A2.

Table A1
Structure mechanical properties.

Dimension (mm)	ρ (kg/m^3)	E (GPa)	ν
$30 \times 600 \times 3.2$	2700	70	0.33

Table A2
Mechanical and electrical properties of the piezoelectric elements (NOLIAC®).

Dimension (mm)	ρ (kg/m^3)	E_{11} (GPa)	E_{33} (GPa)	ν_{12}	d_{31} (pC/N)	d_{33} (pC/N)
$20 \times 30 \times 0.5$	7600	62.50	52.63	0.38	-195	460

References

[1] D. Halim, Control of flexible structures with spatially varying disturbance: spatial H_∞ approach, in: 43rd IEEE Conference on Decision and Control, Atlantis, Paradise Island, Bahamas, 2004, pp. 5065–5070. http://dx.doi.org/10.1109/CDC.2004.1429610.
[2] Y.-R. Hu, A. Ng, Active robust vibration control of flexible structures, J. Sound Vib. 288 (1–2) (2005) 43–56, http://dx.doi.org/10.1016/j.jsv.2004.12.015.

[3] B. Chomette, D. Rémond, S. Chesné, L. Gaudiller, Semi-adaptive modal control of on-board electronic boards using an identification method, *Smart Mater. Struct.* 17 (6) (2008) 1–8, http://dx.doi.org/10.1088/0964-1726/17/6/065019.

[4] M. Marinaki, Y. Marinakis, G.E. Stavroulakis, Fuzzy control optimized by PSO for vibration suppression of beams, *Control Eng. Pract.* 18 (6) (2010) 618–629, http://dx.doi.org/10.1016/j.conengprac.2010.03.001.

[5] S. Khot, N.P. Yelve, R. Tomar, S. Desai, S. Vittal, Active vibration control of cantilever beam by using PID based output feedback controller, *J. Vib. Control* 18 (3) (2011) 366–372, http://dx.doi.org/10.1177/1077546311406307.

[6] C. Shin, C. Hong, W.B. Jeong, Active vibration control of beams using filtered-velocity feedback controllers with moment pair actuators, *J. Sound Vib.* 332 (12) (2013) 2910–2922, http://dx.doi.org/10.1016/j.jsv.2012.12.037.

[7] S. Xiao, Y. Li, Dynamic compensation and H_∞ control for piezoelectric actuators based on the inverse Bouc–Wen model, *Robot. Comput.-Integr. Manuf.* 30 (1) (2014) 47–54, http://dx.doi.org/10.1016/j.rcim.2013.08.002.

[8] N. Mechbal, E.G.O. Nóbrega, Spatial H_∞ approach to damage-tolerant active control, *Struct. Control Health Monit.* 22 (9) (2015) 1148–1172, http://dx.doi.org/10.1002/stc.1729.

[9] N. Mechbal, E.G.O. Nóbrega, Damage tolerant active control: concept and state of the art, in: 8th IFAC Symposium on Fault Detection, Supervision and Safety of Technical Processes, Mexico City, Mexico, 2012, pp. 63–71. http://dx.doi.org/10.3182/20120829-3-MX-2028.00257.

[10] M.J. Balas, Active control of flexible systems, *J. Optim. Theory Appl.* 25 (3) (1978) 415–436, http://dx.doi.org/10.1007/BF00932903.

[11] S.-M. Kim, J.-E. Oh, A modal filter approach to non-collocated vibration control of structures, *J. Sound Vib.* 332 (9) (2013) 2207–2221, http://dx.doi.org/10.1016/j.jsv.2012.12.002.

[12] N. Mechbal, E.G.O. Nóbrega, Adaptive strategy to damage-tolerant active control, in: 9th IFAC Symposium on Fault Detection, Supervision and Safety for Technical Processes, Paris, France, 2015, pp. 658–663. http://dx.doi.org/10.1016/j.ifacol.2015.09.602.

[13] M.J. Balas, Direct velocity feedback control of large space structures, *J. Guid. Control Dyn.* 2 (3) (1979) 252–253, http://dx.doi.org/10.2514/3.55869.

[14] L. Meirovitch, H. Baruh, H. Oz, A comparison of control techniques for large flexible systems, *J. Guid. Control Dyn.* 6 (4) (1983) 302–310, http://dx.doi.org/10.2514/3.19833.

[15] L. Meirovitch, H. Baruh, The implementation of modal filters for control of structures, *J. Guid. Control Dyn.* 8 (6) (1985) 707–716, http://dx.doi.org/10.2514/3.20045.

[16] D.J. Inman, Active modal control for smart structures, *Philos. Trans. R. Soc. Lond. A* 359 (1778) (2001) 205–219, http://dx.doi.org/10.1098/rsta.2000.0721.

[17] E. Omidi, S.N. Mahmoodi, Vibration control of collocated smart structures using H_∞ modified positive position and velocity feedback, *J. Vib. Control* 22 (10) (2014) 2434–2442, http://dx.doi.org/10.1177/1077546314548471.

[18] N. Mechbal, M. Vergé, G. Coffignal, M. Ganapathi, Application of a combined active control and fault detection scheme to an active composite flexible structure, *Mechatronics* 16 (3–4) (2006) 193–208, http://dx.doi.org/10.1016/j.mechatronics.2005.11.007.

[19] J. Schröck, T. Meurer, A. Kugi, Non-collocated feedback stabilization of a non-uniform Euler–Bernoulli beam with in-domain actuation, in: 50th IEEE Conference on Decision and Control and European Control Conference, Orlando, FL, 2011, pp. 2776–2781. http://dx.doi.org/10.1109/CDC.2011.6160929.

[20] H.F.G. Genari, O. Oliveira Neto, E.G.O. Nóbrega, N. Mechbal, G. Coffignal, Robust vibration control of a vertical flexible structure subject to seismic events, in: XVII International Symposium on Dynamic Problems of Mechanics – DINAME 2015, Natal, Brazil, 2015, pp. 1–10.

[21] A. Preumont, *Vibration Control of Active Structures: An Introduction*, 3rd edition, Springer, 2011.

[22] Z. Gosiewski, Z. Kulesza, Virtual collocation of sensors and actuators for a flexible rotor supported by active magnetic bearings, in: 14th International Carpathian Control Conference, Rytro, 2013, pp. 94–99. http://dx.doi.org/10.1109/CarpathianCC.2013.6560518.

[23] C.G. Mastory, N.G. Chalhoub, Enhanced structural controllers for non-collocated systems, *J. Vib. Control* 22 (3) (2014) 678–694, http://dx.doi.org/10.1177/1077546314530418.

[24] X. Tang, I. Chen, Robust control of XYZ flexure-based micromanipulator with large motion, *Front. Mech. Eng. China* 4 (1) (2009) 25–34, http://dx.doi.org/10.1007/s11465-009-0004-2.

[25] B. Chomette, S. Chesné, D. Rémond, L. Gaudiller, Damage reduction of on-board structures using piezoelectric components and active modal control: *application to a printed circuit board*, *Mech. Syst. Signal Process.* 24 (2) (2010) 352–364, http://dx.doi.org/10.1016/j.ymssp.2009.07.010.

[26] H.F.G. Genari, N. Mechbal, G. Coffignal, E. G. O. Nóbrega, A modal H_∞ control methodology for damage-tolerant active control, in: 9th IFAC Symposium on Fault Detection, Supervision and Safety for Technical Processes, Paris, France, 2015, pp. 664–669. http://dx.doi.org/10.1016/j.ifacol.2015.09.603.

[27] A.L. Serpa, E.G.O. Nobrega, H_∞ control with pole placement constraints for flexible structures vibration reduction, in: 18th International Congress of Mechanical Engineering – COBEM2005, Ouro Preto, Brazil, 2005, pp. 1–8.

[28] A. Baz, S. Poh, Experimental implementation of the modified independent modal space control method, *J. Sound Vib.* 139 (1) (1990) 133–149, http://dx.doi.org/10.1016/0022-460X(90)90780-4.

[29] J.Q. Fang, Q.S. Li, J.M. Jeary, Modified independent modal space control of m.d.o.f. systems, *J. Sound Vib.* 261 (3) (2003) 421–441, http://dx.doi.org/10.1016/S0022-460X(02)01085-4.

[30] F. Resta, F. Ripamonti, G. Cazzulani, M. Ferrari, Independent modal control for nonlinear flexible structures: *an experimental test rig*, *J. Sound Vib.* 329 (8) (2010) 961–972, http://dx.doi.org/10.1016/j.jsv.2009.10.021.

[31] M. Serra, F. Resta, F. Ripamonti, Dependent modal space control, *Smart Mater. Struct.* 22 (10) (2013) 1–11, http://dx.doi.org/10.1088/0964-1726/22/10/105004.

[32] S. Cinquemani, D. Ferrari, I. Bayati, Reduction of spillover effects on independent modal space control through optimal placement of sensors and actuators, *Smart Mater. Struct.* 24 (8) (2015) 1–11, http://dx.doi.org/10.1088/0964-1726/24/8/085006.

[33] H.F.G. Genari, N. Mechbal, G. Coffignal, E.G.O. Nóbrega, Damage-tolerant active control using a modal H_∞-norm-based methodology, Control Eng. Pract. (2017), 60, 76–86, http://dx.doi.org/10.1016/j.conengprac.2016.10.018.

[34] P. Ambrosio, G. Cazzulani, F. Resta, F. Ripamonti, An optimal vibration control logic for minimising fatigue damage in flexible structures, *J. Sound Vib.* 333 (5) (2014) 1269–1280, http://dx.doi.org/10.1016/j.jsv.2013.11.010.

[35] F. Ripamonti, G. Cazzulani, S. Cinquemani, F. Resta, A. Torti, Adaptive active vibration control to improve the fatigue life of a carbon-epoxy smart structure, in: Proceedings of SPIE, Active and Passive Smart Structures and Integrated Systems, vol. 9431, 2015, pp. 1–9. http://dx.doi.org/10.1117/12.2084159.

[36] W. Gawronski, *Advanced Structural Dynamics and Active Control of Structures*, Springer-Verlag, 2004.

[37] P. Gahinet, A. Nemirovski, A.J. Laub, M. Chilali, LMI Control Toolbox: For Use with MATLAB®, The MathWorks, 1995.

[38] K. Zhou, J.C. Doyle, *Essentials of Robust Control*, Prentice Hall, 1997.

[39] S. Boyd, L. El Ghaoui, E. Feron, V. Balakrishnan, *Linear Matrix Inequalities in Systems and Control Theory*, SIAM, Philadelphia, 1994.

[40] H. Zheng, A. Mita, Damage indicator defined as the distance between ARMA models for structural health monitoring, *Struct. Control Health Monit.* 15 (2008) 992–1005, http://dx.doi.org/10.1002/stc.235.

[41] H.F.G. Genari, E.G.O. Nóbrega, N. Mechbal, Structural damage diagnosis method based on subspace identification metric, in: 22nd International Congress of Mechanical Engineering, Ribeirão Preto, Brazil, 2013, pp. 4200–4208.

[42] K. De Cock, B. De Moor, Subspace angles between ARMA models, *Syst. Control Lett.* 46 (4) (2002) 265–270, http://dx.doi.org/10.1016/S0167-6911(02)00135-4.

[43] J.L. Batoz, K.J. Bathe, L.W. Ho, A study of three-node triangular plate bending elements, *Int. J. Numer. Methods Eng.* 15 (12) (1980) 1771–1812, http://dx.doi.org/10.1002/nme.1620151205.

[44] A. Preumont, *Vibration Control of Active Structures: An Introduction*, Kluwer Academic Publishers, 2002.